ACS OMEGA

Open Access

http://pubs.acs.org/journal/acsodf

Article

Hetero Sandwich Immunoassay as Tool to Probe the Composition of the Extracellular Vesicles Membranes: The Case Study of L1CAM Localization

Helena Mateos, Antonia Mallardi,* Esther Serrano-Pertierra, Maria Carmen Blanco-López, Maria Liguori, Ylenia Antonacci, Michele Casiello, and Gerardo Palazzo*

Cite This: *ACS Omega* 2025, 10, 12983−12992

Read Online

ACCESS | Metrics & More | Article Recommendations | Supporting Information

ABSTRACT: Lateral flow immunoassays (LFIAs) are widely used for point-of-care diagnostic devices due to their simplicity, low cost, and rapid results. In this work, we demonstrate that a heterosandwich design LFIA can be an effective tool for verifying the presence of different proteins on the same particles. As a case study, we address a recent controversy regarding the presence of the protein L1CAM on the extracellular vesicles (EVs). EVs are crucial for cell communication and may serve as valuable disease biomarkers, including for neurodegenerative disorders. EVs from neuronal cells can cross the blood-brain barrier and be selectively isolated from plasma. Although L1CAM has been suggested as a marker for neuron-derived EVs, recent studies report that L1CAM exists as a cleaved soluble protein in plasma, not associated with EVs. We propose a heterosandwich LFIA to detect and quantify L1CAM and a confirmed EV marker, tetraspanin CD63 or CD9, on the same EV. This assay, together with several control experiments on EVs isolated from plasma by size exclusion chromatography (SEC), demonstrates that although most L1CAM in plasma is present as soluble cleaved proteins, 13% of the EVs are strongly associated with this protein. This evidence is confirmed by dynamic light scattering measurements, showing a significant size increase of gold nanoparticles conjugated with L1CAM antibodies when exposed to EVs but not to cleaved soluble L1CAM. Our results validate the selective immune-isolation of L1CAM-EVs, resolving the controversy by confirming that L1CAM is indeed associated with a significant fraction of EVs despite the presence of its soluble form in plasma.

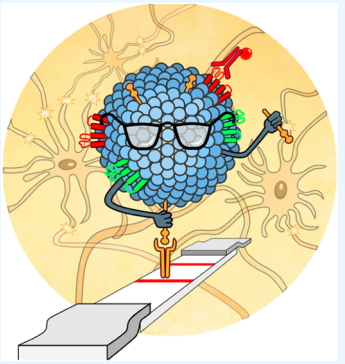

1. INTRODUCTION

Extracellular vesicles (EVs) are membrane structures secreted by cells that act as key mediators in cell−cell communication by transferring their cargo (lipids, nucleic acids, proteins) to recipient cells.[1,2] Recent research has demonstrated that EVs can serve as biomarkers of different diseases, and their cargos can provide information about disease progression.[3,4] Neuron-derived EVs can cross the blood-brain barrier (BBB)[5,6] and are present in body fluids such as the cerebrospinal fluid or plasma. Therefore, the isolation of brain-derived EVs could represent a kind of "liquid biopsy"[7] providing valuable information about conditions or diseases affecting this nearly inaccessible tissue. As an example, EVs have been identified as a carriers of misfolded proteins associated with chronic neurodegenerative diseases such as Alzheimer's disease,[8] dementia,[9] and Parkinson's disease.[10] Additionally, many miRNAs carried by neuronal EVs are differentially expressed during aging and are increasingly recognized as aging biomarkers.[11−14] Research groups around the world have selectively isolated neuronal EVs relying on the L1 cell adhesion molecule (L1CAM, also known as CD171) as a membrane marker.[15,16] L1CAM consists of a long extracellular (ecto)domain composed of six immunoglobulin-like domains linked to five fibronectin type III repeats, a single transmembrane domain, and a short cytoplasmic domain.[17,18] L1CAM has a relatively specific expression in neural tissue. However, in June 2021, Norman et al.[19] published a study claiming that L1CAM is found as soluble protein in plasma and cerebrospinal fluid and therefore, it is not associated with circulating EVs. This affirmation questions the use of L1CAM as a marker for isolating neuron-derived EVs and challenges the numerous studies that have relied on L1CAM to report differences between healthy controls and patients with various neurodegenerative diseases. The state of the debate has been exhaustively discussed in a recent, comprehensive, review[20] which raised four main issues. (i) L1CAM expression is not restricted to neuronal cells; (ii) the crossing of BBB by EVs has only indirect evidence; (iii) one antibody against L1CAM has been reported to cross-react with α-synuclein (an EV cargo protein), potentially invalidating the positive biomarker outcome of some studies; (iv) the

Received: October 14, 2024
Revised: February 16, 2025
Accepted: March 20, 2025
Published: March 25, 2025

association of the L1CAM extracellular moiety with EVs could be transient due to cleavage of the protein ectodomain, resulting in most of the L1CAM found in plasma and cerebrospinal fluid existing as cleaved soluble epitopes. In general, the demonstration and quantification of the presence of specific proteins on the surface of extracellular vesicles are challenging. Specific antibodies with fluorescent tags are often used in combination with sophisticated techniques such as super-resolution optical microscopy, high-resolution flow cytometry or nanoparticle tracking analysis.

To investigate the above-described controversy, we used lateral flow immunoassay (LFIA) technology to test for the presence of L1CAM on the surface of EVs as a transmembrane protein. Nowadays, LFIA is a well-established technology for the rapid, selective, and cost-effective detection of biomarkers in various biological fluids. Blanco-López et al. developed the first LFIA for EVs using tetraspanins or specific markers for capture and detection.[21−24] This approach complements traditional methods for quantifying EVs, offering a simpler and more accessible means to assess the presence and concentration of biomarkers on the surface of EVs. In this work, we developed a heterosandwich LFIA that yields a positive result only when both L1CAM and confirmed EV surface markers are simultaneously present on the same EV. We selected tetraspanins CD9 and CD63, generally accepted as EV surface markers, for this purpose. We isolated EVs from the plasma of 11 healthy volunteers using size exclusion chromatography (SEC) and assayed the obtained fractions with the developed LFIA. The amount of EVs carrying both L1CAM and tetraspanins was measured, indicating that L1CAM is stably present as a protein associated with the membrane of a fraction of plasma circulating EVs, addressing the fourth point mentioned earlier.

2. RESULTS AND DISCUSSION

Figure 1 illustrates the experimental design of the main LFIA platforms used in our investigation, with detailed methods provided in the materials and methods section. The heterosandwich LFIA relies on the recognition of two different antigens on the EV surface by their respective detection or capture antibodies (Abs). The detection Ab is labeled with gold nanoparticles (GNPs) that act as colorimetric (red) reporters. The capture Ab is immobilized on the test line of a nitrocellulose strip and interacts with the respective antigen when the solution (sample + detection Ab) is applied and flows by capillary action. In an optimized assay the capture antibodies are in large excess with respect to the antigens, ensuring that all the EVs are blocked on the test line (that is the first line of Abs that they encounter).

The LFIA platform includes a control line consisting of capture Ab against the detection Abs where the free detection antibodies bind. In the present case, the detection antibody was originated from mouse, so that the control line is composed of antimouse immunoglobulin.

In case of a positive test, EVs labeled by the detection Abs and free detection Abs accumulate in the test and control lines, respectively, resulting in the familiar two red lines response (as in the fast COVID-19 dipstick test). The quantification of EVs is performed by measuring the intensity of the test line with a reflectance reader and comparing it to a calibration curve as proposed elsewhere[21,22] and described in Section S3.1 in the SI.

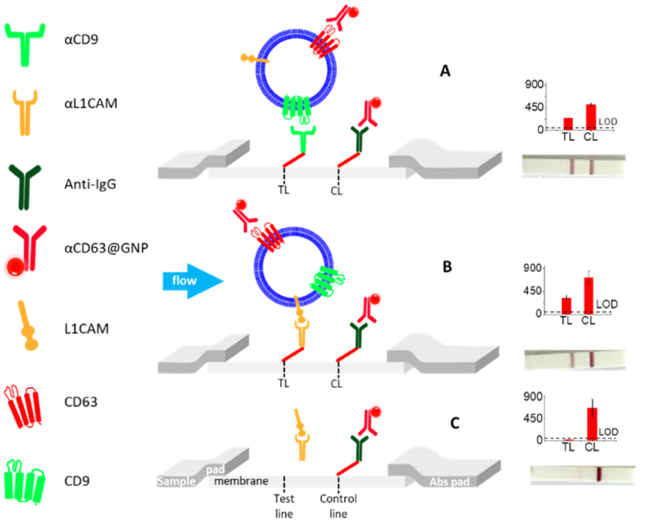

Figure 1. Schematic representation of the LFIA dipstick for EV detection. (A) αCD9/αCD63@GNP configuration with a positive response in the presence of CD9+CD63+EV. Specific antibodies against CD9 tetraspanin are immobilized on the test line (TL). (B, C) αL1CAM/αCD63@GNP configuration with a positive (L1CAM +CD63+EV) and negative (cleaved L1CAM free in solution) response, respectively. Specific antibodies against L1CAM protein are immobilized on the test line. In both configurations, antimouse immunoglobulin antibodies are immobilized on the membrane at control line (CL) and bind the excess detection Abs. EV, if present in the sample, are detected by the detection antibody (αCD63) labeled with GNPs. Adjacent to the schematics, pictures of the LFIA strips are presented along with the measured optical densities at both the TL and CL in the case of: (A) αCD9/αCD63@GNP exposed to plasma-derived EVs; (B) αL1CAM/αCD63@GNP exposed to plasma-derived EVs; (C) αL1CAM/αCD63@GNP exposed to soluble L1CAM.

In our study, we designed two different LFIA configurations, both utilizing the CD63 tetraspanin antibody conjugated with GNP (αCD63@GNP) as the detection Ab. In the first configuration (αCD9/αCD63@GNP), we immobilized the Ab against the CD9 tetraspanin (αCD9) on the test line to detect EVs carrying both CD63 and CD9 tetraspanins (hereafter CD9+CD63+EVs), which likely represents a large fraction of circulating EVs. The rationale for selecting detection and capture Abs is described in detail in refs 21,22. Figure 1A shows that in the αCD9/αCD63@GNP configuration, a positive response is observed only when both CD9 and CD63 are present on the surface of the same EV.

The second configuration introduces an Ab against L1CAM (αL1CAM) on the test line (αL1CAM/αCD63@GNP), proposed for the first time as a time-saving tool to probe the presence of L1CAM on the EV surface. Here, a positive signal will appear only if both L1CAM and CD63 are present on the same EV (L1CAM+CD63+EVs), as shown in Figure 1B. If the sample contains the soluble form of L1CAM, it will be captured and accumulated on the test line but will not produce a positive signal since the detection Ab (αCD63@GNP) only binds to CD63, and not to the L1CAM epitope, therefore only the control line will turn red. This scenario, illustrated on the right of Figure 1C, highlights the assay's specificity, with optical density readings for such samples falling below the limit of quantification and thus indistinguishable from blank samples. Experimentally, we observed that the presence of soluble L1CAM in the concentration range 2 ng/mL−100 μg/

https://doi.org/10.1021/acsomega.4c09363
ACS Omega 2025, 10, 12983−12992

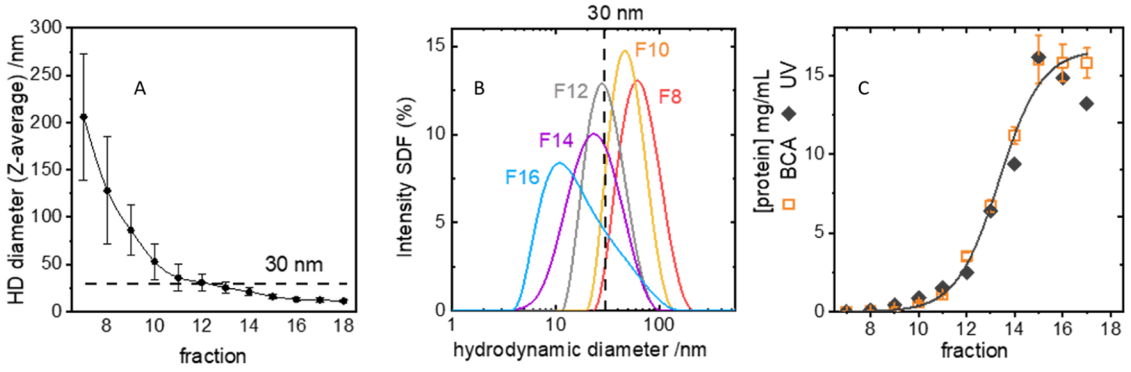

Figure 2. Dynamic Light Scattering of fractions obtained by SEC. (A) Dependence of the Z-averaged HD diameter on fraction number. The dotted line represents the lower dimensional limit of EVs. (B) Particles size distribution of some representative fractions. (C) total protein content evaluated according to the BCA assay (open squares) and UV absorption (closed diamonds).

mL does not induce any positive response in this heterosandwich LFIA.

2.1. Characterization of the SEC Fractions. Given the complex and heterogeneous nature of EVs, a major challenge in the field is confirming their presence with certainty. To ensure that the positive signals observed on the test line of the LFIA are due exclusively to the presence of EVs rather than nonspecific interactions, protein aggregates or contaminants, we used a comprehensive characterization strategy using multiple complementary techniques. EVs were isolated from the plasma of 11 healthy volunteers (5 females and 6 males) using size exclusion chromatography (SEC) to allow direct comparison with the study by Norman et al.[19] For each of the 11 donors, the plasma was fractionated by SEC and fractions 7 to 18 were analyzed for: (i) hydrodynamic (HD) diameter by means of dynamic light scattering (DLS), (ii) total protein content evaluated both through absorbance measurements at 260 and 280 nm and by the bicinchoninic acid (BCA) assay, (iii) The contemporary presence on the same particle of specific EVs' markers, which we define as CD9+CD63+EVs and L1CAM+CD63+EVs using LFIA, and (iv) detection of single or aggregated protein (SAP) contamination using the CONAN assay.[25] Additionally, a subset of plasma samples from three donors was analyzed for phospholipid content, which is a key component of the EV membrane. For this analysis, SEC fractions from the three donors were pooled and subjected to liquid chromatography-mass spectrometry (LC-MS).

This analysis helps differentiate between fractions containing EVs from other particles lacking phospholipids, therefore strengthening our ability to accurately identify EVs in the sample. To quantify human serum albumin (HSA) and total L1CAM protein concentration we used ELISA, while Western blot analysis and transmission electron microscopy (TEM), in accordance with MISEV guidelines, were also employed to further characterize the samples.

Due to polydispersity, the Z-averaged HD diameter obtained from second order cumulant analysis of DLS measurements was used to describe each fraction. Figure 2A illustrates the dependence of this descriptor on the fraction number. The points represent the mean values obtained for the same fraction separated from the plasma of the 11 analyzed subjects, with error bars representing the standard deviation. Fractions 7 to 12 contained particles with a Z-averaged HD diameter ranging from 200 to 30 nm, matching the size of small EVs.[1,20] According to the literature, particles smaller than 30 nm are expected to be nonvesicular extracellular particles (such as exomeres and supermeres) or single or aggregated protein (SAP).[26] However, the size resolution power of SEC is limited, and fractions can contain particles of different sizes. The analysis of DLS allows the retrieval of the size distribution function (SDF) for each fraction (see Section 4.8 for details). Figure 2B displays the SDFs of representative fractions from a given subject. As the fraction number increases, a decrease in average size is observed, but it should be noted that, for fractions above the 12th, the SDF covers a wide range of dimensions and contains a non-negligible number of particles with diameters larger than 30 nm. This result, corroborated by the NTA measurements of Figure S3 of the SI, demonstrates that EVs could be present even in the later fractions, where soluble proteins are mainly eluted.

The protein content of the fractions was routinely assayed using both ultraviolet (UV) spectrometry and the BCA assay, yielding consistent results. As illustrated in Figure 2C, protein content remained below 1 mg/mL up to fraction 11, thereafter increasing dramatically to values well above 10 mg/mL in later fractions. This pattern likely results from the SEC separation process, which confines larger particles, such as the EVs, in the earlier fractions, leaving soluble proteins to accumulate in the later ones. ELISA quantification of soluble HSA, reported in Section S3.2 in SI, showed early fractions of the SEC to be depleted of small soluble proteins such as HSA, which increases significantly in later fractions. The purity of fractions in terms of soluble SAP was assessed using the CONAN assay.[25] This assay specifically targets soluble proteins capable of forming a corona around the nanoparticles used as probes, thereby excluding membrane proteins on the EVs. The data, shown in SI Section S3.3, indicate that fractions above the 12th are heavily enriched with proteins. This general trend holds true across all subjects. The 12th fraction is free from proteins only in some cases (4/11).

All SEC fractions from the plasma of the 11 subjects have been assayed using LFIA with the αCD9/αCD63@GNP configuration, giving a positive result for fraction from 9 to 18. The concentrations of EVs for all fractions of the 11 subjects are listed in the Table S1 in the SI. Figure 3A displays the mean values and standard deviations of EV concentrations (averaged over the cohort of the 11 subjects) as a function of the eluted fractions. The large standard deviations reflect the variability in the number of EVs found in the plasma of different subjects (up to 1 order of magnitude), while still remaining within the average concentration values reported for

https://doi.org/10.1021/acsomega.4c09363
ACS Omega 2025, 10, 12983−12992

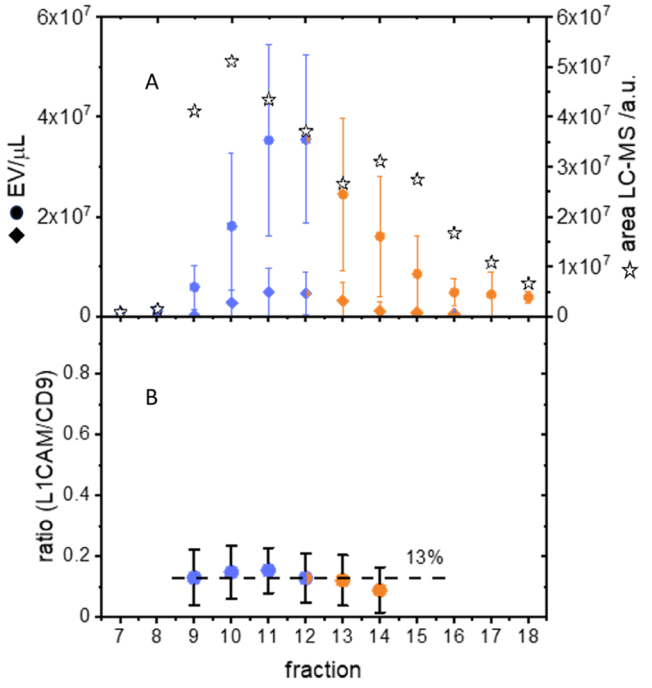

Figure 3. (A) EV quantification by LFIA in SEC fractions from plasma. Full dots indicate the quantification of EVs using LFIA αCD9/αCD63@GNP, while full diamonds represent the quantification of EVs using αL1CAM/αCD63@GNP configuration. Blue and orange symbols represent the fractions that are protein-free, or protein contaminated, respectively. Also shown, as empty stars, are the peak areas of the phosphatidylcholine signal measured by LC-MS (right ordinate). (B) Ratio of L1CAM+CD63+EVs with respect to CD9+CD63+EVs. Each value represents the mean, and the error bars refer to the standard deviation calculated for all 11 subjects studied.

EVs from plasma.[27] The data in Figure 3A demonstrates the presence of CD9+CD63+EVs in all SEC fractions from 9 to 18.

This result has been confirmed by LC-MS analysis, focused on phosphatidylcholines (m/z = 760 and 786, and the corresponding Na+ adducts) as probes for phospholipid presence. These experiments described in detail in the Section S3.5 in SI. The analysis identified four main signals in the mass spectra (see Figure S7 and Table S2) of the SEC fractions as phosphatidylcholine molecules. The assignment was based on isotopic patterns (Figures S8, S9, S12 and S13) and MS2 fragmentation (Figures S10, S11 and S14) agreeing with the nature of fatty acids present in the fractions. The relative abundance of all these species in the fractions, reported in Figure S15 of SI, matches the EV concentrations determined by LFIA. Interestingly, phospholipids are also present in fractions 12 to 18, indicating that EVs (with HD diameters >30 nm, as shown by DLS data) coexist with soluble proteins in these fractions (see Figure 2B).

This is a crucial point, because fractions later than the 10th were previously assumed to contain primarily soluble proteins, and the presence of L1CAM was considered proof of its existence as cleaved protein not associated with EVs.[19]

2.2. Coexistence of EV-Bound and Soluble L1CAM in the SEC Fractions. The same SEC fractions were assayed using the αL1CAM/αCD63@GNP platform to measure the concentration of particles with both CD63 tetraspanin and L1CAM on their surface (L1CAM+CD63+EVs). Figure 3A shows that the amount of L1CAM+CD63+EVs measured in each fraction, although showing a similar trend, is much smaller than that measured for CD9+CD63+EVs.

Figure 3B shows the fraction of L1CAM+CD63+EVs relative to CD9+CD63+EVs, evidencing a constant value of 0.13 ± 0.02 across fractions 9−14, where L1CAM-containing EVs exceeded the assay's limit of quantification. This indicates that the proportion of L1CAM-carrying EVs in plasma remains constant, regardless of the fractions or individuals. Vesicles were visualized by TEM in SEC fractions where L1CAM +CD63+EVs were detected by LFIA, showing sizes and morphology compatible with EVs (see Section S3.6 in SI).

The levels presence of tetraspanin CD63 and L1CAM in pooled SEC fractions (across subjects) was analyzed by Western blot. Moreover, the presence of albumin was also evaluated with Coomassie blue staining, using BSA as a reference standard. Overall, the obtained results, detailed in Section S3.7 of SI, demonstrate the presence of these proteins

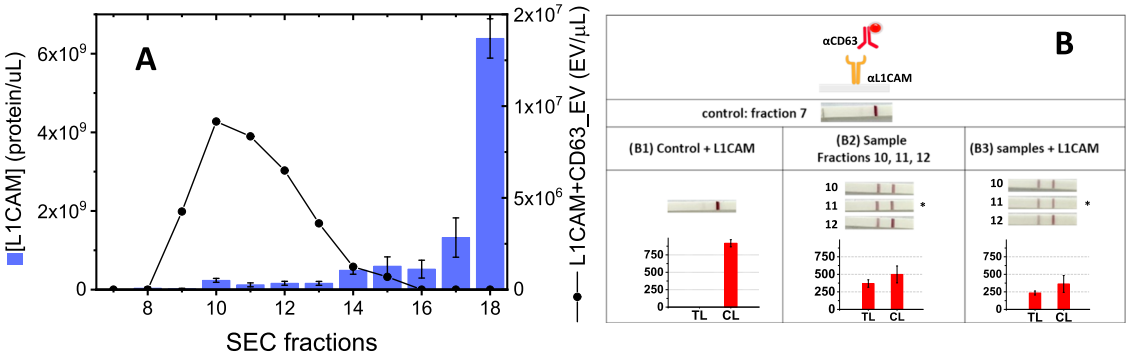

Figure 4. (A) Comparison between total L1CAM protein measured with ELISA (histograms, left ordinate) and L1CAM+CD63+EV content in the SEC fractions (dots, right ordinate). Each measured sample is a pool of the same SEC fraction from three different subjects. The mass of L1CAM measured in the ELISA was converted into proteins/μL considering an average mass of L1CAM of 200 kDa. The measured concentration of L1CAM in fractions 8−13 ranges from 10^7 to10^8 proteins/μL. (B) Representative control experiments performed according to αL1CAM/αCD63@GNP configuration. (B1) LFIA strip of Fraction 7, which is negative for L1CAM+CD63+EV, spiked with soluble recombinant L1CAM. (B2) LFIA strips of fractions 10, 11 and 12, which are positive for L1CAM+CD63+EV. (B3) LFIA strips of the same fractions (10, 11, 12) spiked with soluble recombinant L1CAM, resulting in a reduced signal intensity. signal histograms are shown, with only fraction 11's (*) data shown for clarity. Experiments are performed in triplicates.

https://doi.org/10.1021/acsomega.4c09363
ACS Omega 2025, 10, 12983−12992

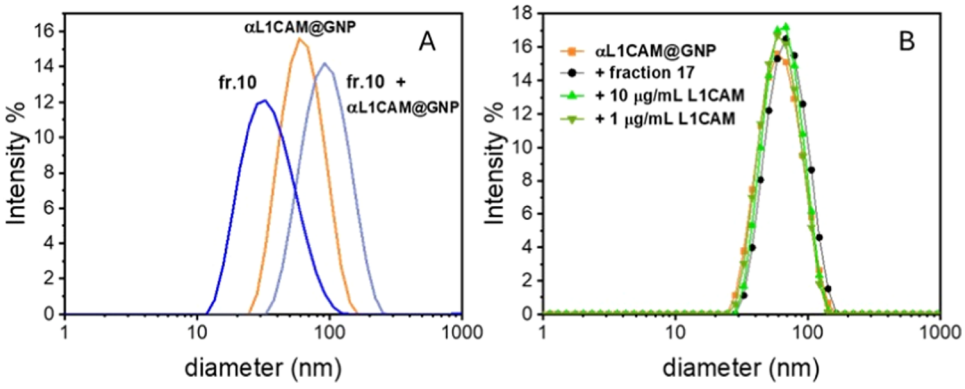

Figure 5. (A) Size distribution of gold nanoparticles conjugated with L1CAM antibodies (αL1CAM@GNP, orange), SEC fraction 10 (blue), and their mixture (gray). (B) Size distribution of αL1CAM@GNPs alone (orange), in the presence of SEC fraction 17 (black), and in the presence of soluble L1CAM at concentrations found in early and late SEC fractions (10 μg/mL dark green and 1 μg/mL light green). All the experiments are performed in PBS solutions.

in fractions 10 to 18, with a substantial enrichment of L1CAM and albumin in the later fractions.

Additionally, all fractions were assayed for total L1CAM protein (both soluble and EV bound) using a commercial ELISA homosandwich assay. Figure 4A shows how the concentration of the L1CAM epitope varies drastically across fractions, being low in earlier fractions and increasing substantially in later ones. According to these data, the content of L1CAM in fractions 7−14 is about 1% of the total L1CAM measured in all fractions up to 18. This observation aligns with findings by Norman et al., who, on the basis of L1CAM distribution across fractions, concluded that L1CAM is not associated with EVs.[19]

In Figure 4A, we also show the concentration of L1CAM +CD63+EVs measured across eluted fractions. Despite the predominance of soluble L1CAM in plasma, there is a distinct part of L1CAM associated with EVs, which, in turn, are efficiently captured and measured using anti-L1CAM antibodies by LFIA.

This finding could reconcile the large amounts of soluble L1CAM found in plasma with the effectiveness of EV-isolation procedures based on L1CAM antibodies.

2.3. L1CAM Bound to EVs: LFIA Validation. To validate that the positive signals observed in our heterosandwich αL1CAM/αCD63@GNP platform are due to the presence of L1CAM bound to EVs, we conducted a series of control experiments to exclude potential false positives or artifact-induced responses due to the possible presence of soluble L1CAM in the samples.

The first experiments included isotype (negative) controls using two different capture antibodies that matched the isotype of the mouse anti-L1CAM (IgG1). We tested two antibodies without specific affinity to any antigen in the sample: a mouse IgG1 antibody against mycotoxin (Clone mab22)[28] and a commercially available mouse IgG1 antibody against synthetic hapten. The absence of nonspecific binding for EVs was confirmed by the negative results of these assays, as detailed in Section S3.8 of the SI.

To further rule out potential cross-reactivity between the capture antibody αL1CAM and EV-membrane proteins other than L1CAM, the procedure was replicated using rabbit-purified αL1CAM as capture antibody to test fractions from four subjects. The assay results were identical to those obtained using the mouse antibody, within experimental error (see Section S3.9 in SI). evidencing the specificity of the assay for EV-bound L1CAM. The rabbit-purified αL1CAM and the mouse-purified αL1CAM have completely different colloidal stabilities[29] suggesting large structural differences. It is highly improbable for two antibodies generated in two different organisms through immunization with the same purified recombinant Human L1CAM to have the same affinity for EV-associated proteins that are not the natural antigen.

To address the concern that soluble L1CAM, not associated with EVs, could produce a false positive in the LFIA, we conducted several control experiments using αL1CAM/αCD63@GNP configuration. Figure 1C schematically illustrates our hypothesis that soluble L1CAM alone would not generate a positive signal on the test line. To validate our hypothesis, we performed spike-in experiments.

Representative results, shown in Figure 4B, use fraction 7 as a control due to its negligible content of EVs. The addition of soluble recombinant L1CAM protein (0.5 mg/mL) to fraction 7 did not elicit a positive response on the αL1CAM/αCD63@GNP test line (Figure 4B1), thereby confirming experimentally that soluble L1CAM does not cause a false positive. We further tested whether the simultaneous presence of nonassociated soluble L1CAM and EVs would affect the LFIA result. To do this, we spiked fractions 10, 11, and 12 (known from Figure 3A to be rich in EVs) with soluble L1CAM protein. The results, shown in Figure 4B2,B3, indicate a decrease in test line intensity by about 30%. This reduction occurs because soluble L1CAM competes with EV-bound L1CAM for the capture antibodies on the test line, thereby reducing the number of EVs labeled with detection antibodies (αCD63@GNP) that are immobilized on the test line,which in turn decreases the signal.

All these control experiments corroborate the coexistence of L1CAM and CD63 on the same EV.

For selected samples, we used αCD9 as capture antibody and αL1CAM as detection antibody (αCD9/αL1CAM@GNP). This approach yielded positive results, as reported on Section S3.10 of the SI, corroborating the presence of L1CAM on EVs carrying CD9 tetraspanins.

2.4. L1CAM Bound to EVs: DLS Validation. To add further evidence to our study, we measured the size of gold nanoparticles conjugated with L1CAM antibodies (αL1CAM@GNP) in the presence of L1CAM+CD63+EVs and/or cleaved soluble L1CAM using DLS.

https://doi.org/10.1021/acsomega.4c09363
ACS Omega 2025, 10, 12983−12992

Figure 5A shows the size distribution of both αL1CAM@GNP and SEC fraction n. Ten (positive to the αL1CAM/αCD63@GNP LFIA and thus containing L1CAM+CD63+EVs), before and after mixing. The αL1CAM@GNP are characterized by a size distribution centered at 55 nm, accounting for the metallic core size of 40 nm + the antibody shell thickness of about 7 nm. Fraction 10 has a monomodal size distribution with a maximum at 33 nm and, as discussed in Section 2.1, includes particles up to 100 nm, compatible with the presence of EVs.

Due to the significant scattering power of the GNPs compared to EVs, this experiment primarily measures the diffusion coefficient of the GNPs. The diffusion coefficient of GNPs will be lower if the conjugated αL1CAM binds to large EVs, resulting in larger hydrodynamic sizes.

Figure 5A also shows that when αL1CAM@GNP is added to fraction 10, the size distribution shifts toward larger diameters, with a maximum above 100 nm. This shift indicates the binding of αL1CAM@GNP to L1CAM protruding from the EVs surface.

Note that the experiments are performed in PBS solution where the αL1CAM@GNP are stable and do not aggregate (orange trace in Figure 5A). Indeed, the Ab protein corona stabilizes the GNP at a NaCl concentration of at least 0.68 M (more than a 4-fold the PBS ionic strength) as explained in the Section 4.

To demonstrate that the observed size increase is not due to binding to soluble L1CAM, control experiments were performed. Figure 5B compares the size distribution functions of αL1CAM@GNPs alone and in the presence of soluble L1CAM at concentrations found by ELISA assay in early fractions rich in EVs ([L1CAM] = 1 μg/mL) and in late fractions rich in proteins ([L1CAM] = 100 μg/mL). The three SDFs are indistinguishable, evidencing that binding of soluble L1CAM to αL1CAM@GNPs does not affect the GNPs' hydrodynamic size. Further confirmation comes from mixing αL1CAM@GNPs with SEC fraction 17, which is negative in the αL1CAM/αCD9@GNP LFIA (it does not contain L1CAM-bound EVs as shown in Figure 3A). As shown in Figure 5B, also in this case the SDF remains unperturbed with respect to that of the pristine αL1CAM@GNPs, confirming that the size increase observed for fraction 10 is due to the specific binding of αL1CAM@GNPs to L1CAM associated with EVs and not to binding to soluble L1CAM or to nonspecific binding with other proteins on the EV surface.

3. CONCLUSIONS

We analyzed plasma samples from 11 healthy subjects using custom-developed heterosandwich LFIA platforms. EVs containing CD9 and CD63 tetraspanins are present in fractions 9−18 eluted from the SEC column. The presence of EVs, even in the later fractions, can be attributed to the limited resolution of SEC in terms of size separation. Using an analogous approach, we have identified EVs containing both CD63 and the L1CAM protein in fractions 9−14. The nature of the assay confirms that L1CAM in these fractions is associated with EVs rather than being present as a soluble protein. This evidence has been independently proved by DLS showing a significant size increase of GNP conjugated with αL1CAM when exposed to EVs but not to cleaved soluble L1CAM. Based on the findings here presented, we conclude that while most of the plasma L1CAM is present in a soluble form (likely as cleaved epitope) a non-negligible (13%) fraction plasma EVs containing CD63 and CD9 is effectively associated with L1CAM and can be efficiently isolated using L1CAM antibodies. Additionally, this study represents the first time of employing heterosandwich LFIA as a low-cost and time saving method to probe the composition of the EV membranes, and this strategy can be extended also to other membrane proteins. This approach can be extended to any marker, provided that antibodies are available and the concentration of the associated EVs is high enough to fulfill the LOQ of the LFIA. For markers present at very low concentrations, as in some disease-related EVs, a preconcentration step may be necessary to achieve reliable detection.

4. EXPERIMENTAL SECTION

4.1. LFIA Materials. Citrate capped gold nanoparticles (GNPs) with a nominal diameter of 40 nm and a concentration of 1.5×10^{-10} M have been purchased from BBI Solutions—U.K.

The recombinant anti-L1CAM antibody Rabbit Monoclonal, hereafter referred to as rabbit-αL1CAM, was purchased from Sino Biological Europe GmbH—Germany (catalogue number 10140-R001). It was obtained from a rabbit immunized with purified, recombinant Human L1CAM protein and stored in a 0.2 μm filtered solution in PBS at 1 mg/mL.

The recombinant anti-L1CAM antibody Mouse Monoclonal, referred to as mouse-αL1CAM, was purchased from Sino Biological Europe GmbH—Germany (catalogue number 10140-MM01) (Sino Biological Cat# 10140-R014, RRID:AB_2860093).

It was obtained from a hybridoma resulting from the fusion of a mouse myeloma with B cells obtained from a mouse immunized with purified, recombinant Human L1CAM. It is also stored in a 0.2 μm filtered solution in PBS at 1 mg/mL.

The anti-CD9 VJ1−20, referred to as αCD9, was purchased from Sino Biological Europe GmbH − Germany (PURE Bulk catalogue number 9PU).

The anti-CD63 mouse monoclonal antibody, referred to as αCD63, was purchased from Immunostep Salamanca-Spain (catalogue number 63PU) as a 1 mg/mL solution in PBS.

The antimouse IgG, produced in goat, was purchased from SIGMA (COD M8642).

The water-soluble L1CAM Protein, Human, Recombinant (Cod 10140-H08H) was purchased from Sino Biological Europe GmbH—Germany. The expected molecular weight, including glycosylation, is 200 kDa.

The antihapten Mouse IgG1 Isotype antibody was purchased by Immunostep.

The antimycotoxin Mouse IgG1 (clone MAB#22) Isotype antibody was a generous gift of Dr. Chris Maragos of the National Centre for Agricultural Utilization Research. Details can be found in ref 28.

The LFIA strips were assembled using a nitrocellulose membrane purchased from MDI Advanced Microdevices PVT (Ambala Cantt, India) (25 mm wide and 15 μm pore size, ref 70CNPH-N-SS40). The cellulose sample pad (10 mm wide), glass fiber membrane (GFCP001000), and absorbent pads (22 mm wide) were from Millipore (Darmstad, Germany) and Whatman (Piscat- away, NJ), respectively. The different parts of the strips were manually assembled using backing cards (6×30 cm^2) from Millipore (Darmstad, Germany).

4.2. EVs Isolation. Human peripheral blood was collected from 11 healthy volunteers in EDTA-treated tubes. Plasma was

https://doi.org/10.1021/acsomega.4c09363
ACS Omega 2025, 10, 12983−12992

obtained after a 15 min centrifugation at 3000*g*. Plasma samples were aliquoted and stored at −20 °C until further use. Plasma samples were thawed at room temperature and centrifuged at 2000*g* for 2 min at 4 °C to remove any aggregates due to thawing. Subsequently, EVs were isolated by SEC using qEV Columns (IZON, qEV original 35 nm) following the manufacturer instructions. Briefly, columns were washed with at least 10 mL of PBS. The column was allowed to completely drip out before introducing 0.5 mL of the plasma sample. Once the plasma had fully passed through the frit, PBS was incrementally added to the column's top in 0,5 mL portions which were subsequently collected in 0,5 mL fractions. In this case, fraction 1 refers to the eluent collected immediately after the addition of the plasma sample. Fractions 7−18 were collected.

4.3. Preparation of Immunostrips. An IsoFlow reagent dispensing system (Imagene Technology, USA) was used to dispense the antibodies on the detection and control lines at a rate of 0.100 mL/mm. The concentration of the antibody solutions dispensed on the test line (with rabbit or mouse αL1CAM or αCD9) and control lines (anti-IgG) were 1 mg/mL. The nitrocellulose membrane was then dried overnight at room temperature to ensure the immobilization of the antibodies. The membrane was placed on a backing card with the sample and absorbent pads overlapping by 2 mm. Subsequently, the complete card was cut into separate 4 mm dipstick strips using a guillotine Fellowes G amma (Spain).

The minimum detection antibody (αCD63 or αL1CAM) concentration needed for the stabilization of GNPs was determined using the protocol described in ref 30. The samples were directly prepared in multiwell plates. Briefly, 20 μL of increasing anti-CD63 antibody concentrations (final concentrations ranging from 0.1 to 20 μg/mL) in 10 mM phosphate buffer (PB) at pH 7,5 were added to 250 μL of 1.5×10^{-10} M GNP suspensions. The mixtures of GNP-antibody were allowed to equilibrate for 30 min, after which 100 μL of 1.85 M NaCl in 10 mM PB were added to the samples (the final NaCl concentration was 0.68 M). The antibody concentration that resulted in a stable solution of nanoparticles was determined to be 10 μg/mL and selected for the conjugation protocol. Next, 100 μL of the anti-CD63 solution were combined with 1.5 mL of the GNP suspension (1.5×10^{-10} M) to achieve a final concentration of 10 μg/mL. The mixture was gently mixed for 1 h. Following that, 100 μL of blocking solution (1 mg/mL BSA in 10 mM PB, pH 7.4) were added to block any remaining surfaces of antibody-colloidal gold conjugates. After a 45 min reaction, the mixture was divided in two and centrifuged at 10,000 rpm for 20 min at room temperature. 700 μL of the supernatant were discarded, and the resulting pellet was resuspended in 100 μL of the stabilization solution, prepared as 10% sucrose, 1% BSA in PB 2 mM. The GNPs-anti-CD63 conjugates (αCD63@GNP) were then stored at 4 °C until further use.

4.4. LFIA Procedure. For the test we use a running buffer, previously optimized to minimize nonspecific binding and enhance signal intensity, consisting of 10 mM HEPES pH 7.5, 100 mM NaCl, 0.05% Tween-20 and 1% BSA. The immunostrips were vertically immersed in a *running solution* containing a small aliquot (usually 1 μL) of the SEC fractions, 10 μL of the GNP-anti-CD63 solution and the running buffer up to a total volume of 100 μL. The strips were allowed to run 20 min before reading the results.

A strip reader ESE Quant LR3 lateral flow system (Qiagen Inc., Germany) was used to quantify the intensity of the test line by reflectance measurements. The dead volume of the SEC column (first eluted 4 mL) was used as negative control (blank). The quantification of EVs is performed by comparing the intensity of the test line to a calibration curve as proposed elsewhere[21,22] and described in Section S3.1 in the SI. The reference solution used for the calibration curve is a pool of fractions 9, 10, and 11 from three different subjects.

In those SEC fractions where the intensity of the test line exceeded the upper limit of the calibration curve, the samples were suitable diluted prior to the LFIA. When the reading was below 10 times the signal-to-noise ratio of the blank, meaning the concentration in the running solution is below the limit-of-quantification (LOQ), a larger sample volume was mixed with the running buffer to obtain the 100 μL of the *running solution*. In any case, the actual volume of the sample loaded was taken into account for the final concentration calculation (see Supporting Information Section S3.1 for details).

4.5. ELISA for HSA and L1CAM Determination. The Albumin Human ELISA Kit (Cat. N. EHALB) and the Human L1CAM ELISA Kit (Cat. N. EH290RB), both from Invitrogen, were performed on SEC fractions, following the manufacturer's recommendations. Each measured sample is a pool of the same SEC fraction from three different subjects.

4.6. Bicinchoninic Acid Assay. For analysis of protein concentration in SEC fractions, the Pierce BCA Protein Assay Kit (Thermo Fisher Scientific) was performed, following the manufacturer's recommendations.

4.7. Colorimetric Nanoplasmonic (Conan) Test of EVs Purity. The protein depletion of SEC fractions was assessed by means of the Conan assay based on the interaction between EVs and GNPs. The procedure and the physical basis of the method are reported in the paper by Zendrini et al.;[25] and are summarized below.

In the presence of pure EVs, GNPs adsorb and cluster at their lipid membrane. This results in a redshift of the plasmonic absorption, as well as in a change in the color of the solution from pink to blue. Should be noted that, in the case of a very concentrated EV preparation, the amount of GNPs per vesicle is not enough to come into contact and the GNPs adsorbed on the vesicle lipid membrane are so far apart that clustering is negligible. GNP aggregation is also prevented in the presence of single and aggregated proteins (SAP) that are able to adsorb on the surface of GNPs, forming a nanoparticle−protein corona complex. In both situations, the surface plasmon resonance peak remains unchanged with respect to that of the water dispersed GNPs, and the solution remains pink. As the color pink of the solution can be due to either the presence of proteins or a high concentration of EVs, consecutive dilutions of the sample are prepared to distinguish between these two situations. In fact, in the absence of protein contamination, dilutions of EVs will allow the clustering of GNPs at the EV surface, and the solution will turn blue. According to this hypothesis, if none of the dilutions turns blue, the sample is contaminated.

For the assay, 200 μL of a suitable dilution of the SEC fraction (usually 1 μL of sample +199 μL of water) were incubated with 300 μL of GNPs (synthesized following the Turkevich method,[31] at initial concentration of 4.5 nM) and 100 μL of PBS, for 10 min at room temperature. The UV−visible (UV−vis) spectrum of solutions was collected in the region between 400 and 900 nm using an Agilent 8453 UV−

https://doi.org/10.1021/acsomega.4c09363
ACS Omega 2025, 10, 12983−12992

vis diode-array spectrophotometer and the GNPs aggregation was calculated using the aggregation index value (AI). This value is the ratio of the extinction peak of monodispersed GNPs in water to the sum of the extinction at 650 and 850 nm (indicative of the red-shift wavelength)

$$\mathrm{AI} = \frac{\mathrm{Abs@maximum}}{\mathrm{Abs@650} + \mathrm{Abs@800}}$$

The relative aggregation index, AI (%) is then evaluated as the ratio (%) of the sample AI to the AI of untreated monodispersed GNPs

$$\mathrm{AI}\ (\%) = (\mathrm{AI\ sample}/\mathrm{AI\ GNPs})\%$$

AI (%) ≤ 20% corresponds the SAP limit of detection (LOD) value, corresponding to a SAP concentration of 0.05 mg/mL. Therefore, EV samples showing an $AI_{ratio} \leq 20$ can be considered highly pure. The assay also requires the preparation of an "internal reference" sample (obtained mixing 200 μL of water with 300 mL of GNPs and 100 mL of PBS) whose AI (%) defines the threshold below which the GNP aggregation is due to the interaction between GNPs and EVs with a very low SAP content. Therefore, samples (possibly after dilution) with an AI (%) lower than the internal reference AI (%) can be considered pure while a AI (%) higher of the internal reference (also after sample dilution) means that sample is SAP contaminated.

4.8. Dynamic Light Scattering (DLS). Measurements were conducted in disposable plastic cuvettes using a Zetasizer-Nano ZS from Malvern. The instrument operated with a 4 mW He−Ne laser (633 nm wavelength) and a fixed detector angle of 173° (NIBS). The parameters (attenuator, optics position, and number of runs) were optimized by the instrument during data collection. Typically, the time autocorrelation function (ACF) of scattered light intensity was obtained by averaging 12−16 consecutive runs, each lasting 10 s. The ACF of scattered light intensity was then converted into the ACF of scattered electric field. To estimate the average hydrodynamic size, the ACF of the electric field was fitted using a second-order cumulant expansion. This estimation is known as the z-averaged hydrodynamic (HD) diameter and represents an average over all particles in solution.[32] In addition, the analysis of the ACF allows to retrieve the intensity-weighted size distribution function (SDF) of the particles in solution by inversion of Laplace transform of the ACF using a standard regularized non-negative least-squares analysis implemented by the manufacturer's software. The resulting intensity-weighted size distribution function provides information about the fraction of light intensity scattered by particles of different sizes.

4.9. TEM. Two consecutive SEC fractions from the plasma of three different donors have been pooled. EV samples were deposited onto a carbon-coated copper grid and negatively stained for 1 min with 2% uranyl acetate. Samples were analyzed using a JEOL 1011 electron microscope (JEOL Ltd., Tokyo, Japan) operated at 100 kV.

4.10. Western Blot and SDS-PAGE Analysis. EV samples from pooled SEC fractions, from three different donors, were first concentrated by ultrafiltration then mixed with reducing or nonreducing 5× LaemmLi buffer and boiled for 5 min at 95 °C. Samples were run on 8% or 10% SDS-PAGE gels and transferred to PVDF membranes (Amersham; GE Healthcare, Munich, Germany). Membranes were blocked with 5% skimmed milk in T-TBS and incubated overnight at 4 °C with anti-L1CAM (1:1000) and anti-CD63 (1:500, Santa Cruz Biotech; CA). Membranes were then washed and incubated with IRDye 800CW goat antimouse secondary antibody (LI-COR Biosciences GmbH, Germany; 1:10,000) and then visualized with LI-COR Odyssey Imaging System (LI-COR Biosciences GmbH, Germany).

The global protein content was analyzed by Coomassie blue staining.

4.11. Nanoparticle Tracking Analysis. The size distribution of EVs and their absolute concentration was determined by means of Nanoparticle Tracking Analysis (NTA) using a NanoSight NS300 instrument (Malvern, Worcestershire, U.K.) and NTA 3.3 software

4.12. Phospholipids Analysis. HPLC grade solvents, chemicals and TBAI (tetrabutylammonium iodide) were purchased from Sigma-Aldrich and ZnO was purchased from Carlo Erba. All the reagents were used as received. Each measured sample is a pool of the same SEC fraction from three different subjects.

The distribution of fatty acids in the lipids was determined by transesterification/hydrolysis reactions carried out in a Pyrex vial sealed with a Sovirel cap and equipped with a magnetic bar. 0.4 mL of each SEC fractions from n. Seven to n.18, were pooled to a total volume ∼5 mL and left to react for 6 h in the presence of 10 mL of methanol, 3 mg of ZnO and 70 mg of TBAI at 70 °C.[33] After completion, the reaction mixture was cooled to room temperature, transferred into a centrifuge tube, and centrifuged at 3500 rpm for 15 min. A white solid ZnO layered at the bottom, and an upper methanol/water phase was subjected to workup for the extraction of esters and free fatty acids, which were subsequently characterized by GC-MS using a Shimadzu GC 17-A linked to a Shimadzu GC/MS QP5050A selective mass detector (capillary column: HP-5 MS, 30 m).

Identification of phospholipids present in the different SEC fractions was carried out using a HPLC-MS IT-TOF Shimadzu equipped with ESI interface by direct infusion. 400 μL of each sample were diluted in 1.5 mL of a CH_3OH/H_2O solution (1:2), then 5 μL were direct injected into the instrument. The liquid carrier employed was an isocratic mixture of $CH_3OH/H_2O/CH_3CN$ (2:4:1) set at a flow rate of 0.2 mL per minute. The ESI interface was set at a temperature of 200 °C. The measurement range of the masses was set from 500 to 1000 m/z, while the precursor fragments were sampled from 100 to 1000 m/z. The nebulizing gas (nitrogen) was regulated with a flow of 1.5 L/min. Mass spectra MS^1 and MS^2 were recorded for both the positive and negative channels. Mass Spectra were elaborated with LCMS solution software suite (V3.80.410) (Shimadzu).

■ ASSOCIATED CONTENT

Supporting Information

The Supporting Information is available free of charge at https://pubs.acs.org/doi/10.1021/acsomega.4c09363.

Declaration of approval for human plasma experiments; EV-TRACK knowledgebase submission; calibration curve; nanoparticle tracking analysis; ELISA determination of HSA in the SEC fractions; CONAN assay; GLC-MS characterization of fatty acids in phospholipids; TEM; Western Blot; isotype controls; LFIA

https://doi.org/10.1021/acsomega.4c09363
ACS Omega 2025, 10, 12983−12992

experiments using rabbit-purified αL1CAM; LFIA experiments with αL1CAM@GNP (PDF)

AUTHOR INFORMATION

Corresponding Authors

Antonia Mallardi − *CNR-IPCF, Institute for Physical and Chemical Processes—Bari Division, National Research Council (CNR), 00185 Rome, Italy*; Email: antonia.mallardi@cnr.it

Gerardo Palazzo − *Dipartimento di Chimica and CSGI (Center for Colloid and Surface Science), Università degli Studi di Bari "Aldo Moro", 70125 Bari, Italy*; orcid.org/0000-0001-5504-2177; Email: gerardo.palazzo@uniba.it

Authors

Helena Mateos − *Dipartimento di Chimica and CSGI (Center for Colloid and Surface Science), Università degli Studi di Bari "Aldo Moro", 70125 Bari, Italy*

Esther Serrano-Pertierra − *Departamento de Bioquímica y Biología Molecular & Instituto Universitario de Biotecnología de Asturias, Universidad de Oviedo, 33006 Oviedo, Spain*; orcid.org/0000-0001-8356-858X

Maria Carmen Blanco-López − *Departamento de Química Física y Analítica & Instituto Universitario de Biotecnología de Asturias, Universidad de Oviedo, 33006 Oviedo, Spain*; orcid.org/0000-0002-9776-9013

Maria Liguori − *CNR-ITB, Institute of Biomedical Technologies—Bari Unit, National Research Council (CNR), 70125 Bari, Italy*

Ylenia Antonacci − *CNR-ITB, Institute of Biomedical Technologies—Bari Unit, National Research Council (CNR), 70125 Bari, Italy*

Michele Casiello − *Dipartimento di Chimica and CSGI (Center for Colloid and Surface Science), Università degli Studi di Bari "Aldo Moro", 70125 Bari, Italy*; orcid.org/0000-0002-0836-9318

Complete contact information is available at: https://pubs.acs.org/10.1021/acsomega.4c09363

Funding

This work was funded by the Ministerio de Ciencia y Tecnología, grant number MCI-21-PID2020−119087RB-I00, and Consejería de Educación y Ciencia del Principado de Asturias (refSV-PA-21-AYUD/2021/52132) and Italian Ministry of University and Research (MUR) within the NextGeneration EU-MUR PNRR initiative: Extended Partnership on Emerging Infectious Diseases (Project no. PE00000007, INF-ACT) and PRIN 2022 PNRR grant number P2022ZAHJY. H.M. was funded by University of Bari under the program ERC SEEDS UNIBA"—grant number 2023-UNBACLE-0243485.

Notes

The authors declare no competing financial interest.

ACKNOWLEDGMENTS

The Authors would like to thank the healthy subjects who voluntarily provided their peripheral blood samples for the analysis. All subjects signed written informed consent forms (according to the Declaration of Helsinki) at the time of the enrollment. The study was approved by the local Ethic Committee of IRCCS Istituto Oncologico "Gabriella Serio", Bari (protocol number: 388/2023).

REFERENCES

(1) Théry, C.; Witwer, K. W.; Aikawa, E.; Alcaraz, M. J.; Anderson, J. D.; Andriantsitohaina, R.; Antoniou, A.; Arab, T.; Archer, F.; Atkin-Smith, G. K.; Ayre, D. C.; Bach, J. M.; Bachurski, D.; Baharvand, H.; Balaj, L.; Baldacchino, S.; Bauer, N. N.; Baxter, A. A.; Bebawy, M.; Zuba-Surma, E. K.; et al. Minimal information for studies of extracellular vesicles 2018 (MISEV2018): a position statement of the International Society for Extracellular Vesicles and update of the MISEV2014 guidelines. *J. Extracell. Vesicles* **2018**, *7*, No. 1535750.

(2) Yates, A. G.; Pink, R. C.; Erdbrügger, U.; Siljander, P. R.; Dellar, E. R.; Pantazi, P.; Akbar, N.; Cooke, W. R.; Vatish, M.; Dias-Neto, E.; Anthony, D. C.; Couch, Y. In sickness and in health: The functional role of extracellular vesicles in physiology and pathology in vivo. *J. Extracell. Vesicles* **2022**, *11*, No. e12151.

(3) Manu, M. S.; Hohjoh, H.; Yamamura, T. Extracellular Vesicles as Pro- and Anti-inflammatory Mediators, Biomarkers and Potential Therapeutic Agents in Multiple Sclerosis. *Aging Dis.* **2021**, *12*, 1451−1461.

(4) Campbell, L. A.; Mocchetti, I. Extracellular vesicles and HIV-associated neurocognitive disorders: Implications in neuropathogenesis and disease diagnosis. *Neurotoxic. Res.* **2021**, *39*, 2098−2107.

(5) Alvarez-Erviti, L.; Seow, Y.; Yin, H.; Betts, C.; Lakhal, S.; Wood, M. J. A. Delivery of siRNA to the mouse brain by systemic injection of targeted exosomes. *Nat. Biotechnol.* **2011**, *29*, No. 306.

(6) Dickens, A. M.; Tovar-Y-Romo, L. B.; Yoo, S. W.; Trout, A. L.; Bae, M.; Kanmogne, M.; Megra, B.; Williams, D. W.; Witwer, K. W.; Gacias, M.; Tabatadze, N.; Cole, R. N.; Casaccia, P.; Berman, J. W.; Anthony, D. C.; Haughey, N. J. Astrocyte-shed extracellular vesicles regulate the peripheral leukocyte response to inflammatory brain lesions. *Sci. Signal.* **2017**, *10*, No. eaai7696.

(7) Martín-Gracia, B.; Martín-Barreiro, A.; Cuestas-Ayllón, C.; Grazú, V.; Line, A.; Llorente, A.; de la Fuente, J. M.; Moros, M. Nanoparticle-based biosensors for detection of extracellular vesicles in liquid biopsies. *J. Mater. Chem. B* **2020**, *8*, 6710−6738.

(8) Lee, S.; Mankhong, S.; Kang, J. H. Extracellular Vesicle as a Source of Alzheimer's Biomarkers: Opportunities and Challenges. *Int. J. Mol. Sci.* **2019**, *20*, No. 1728.

(9) Gámez-Valero, A.; Beyer, K.; Borràs, F. E. Extracellular vesicles, new actors in the search for biomarkers of dementias. *Neurobiol. Aging* **2019**, *74*, 15−20.

(10) Upadhya, R.; Shetty, A. K. Extracellular vesicles for the diagnosis and treatment of Parkinson's disease. *Aging Dis.* **2021**, *12*, 1438−1450.

(11) Hill, A. F. Extracellular vesicles and neurodegenerative diseases. *J. Neurosci.* **2019**, *39*, 9269−9273.

(12) Vandendriessche, C.; Bruggeman, A.; Van Cauwenberghe, C.; Vandenbroucke, R. E. Extracellular vesicles in Alzheimer's and Parkinson's Disease: Small entities with large consequences. *Cells* **2020**, *9*, No. 2485.

(13) Vandendriessche, C.; Balusu, S.; Van Cauwenberghe, C.; Brkic, M.; Pauwels, M.; Plehiers, N.; Bruggeman, A.; Dujardin, P.; Van Imschoot, G.; Van Wonterghem, E.; Hendrix, A.; Baeke, F.; De Rycke, R.; Gevaert, K.; Vandenbroucke, R. E. Importance of extracellular vesicle secretion at the blood−cerebrospinal fluid interface in the pathogenesis of Alzheimer's disease. *Acta Neuropathol. Commun.* **2021**, *9*, No. 143.

(14) Korvenlaita, N.; Gómez-Budia, M.; Scoyni, F.; Pistono, C.; Giudice, L.; Eamen, S.; Loppi, S.; de Sande, A. H.; Huremagic, B.; Bouvy-Liivrand, M.; Heinäniemi, M.; Kaikkonen, M. U.; Cheng, L.; Hill, A. F.; Kanninen, K. M.; Jenster, G. W.; van Royen, M. E.; Ramiro, L.; Montaner, J.; Batkova, T.; Mikulik, R.; Giugno, R.; Jolkkonen, J.; Korhonen, P.; Malm, T. Dynamic release of neuronal extracellular vesicles containing miR-21a-5p is induced by hypoxia. *J. Extracell. Vesicles* **2023**, *12*, No. 12297.

(15) Mustapic, M.; Eitan, E.; Werner, J. K., Jr.; Berkowitz, S. T.; Lazaropoulos, M. P.; Tran, J.; Goetzl, E. J.; Kapogiannis, D. Plasma Extracellular Vesicles Enriched for Neuronal Origin: A Potential Window into Brain Pathologic Processes. *Methods* **2017**, *11*, No. 278.

(16) Pulliam, L.; Sun, B.; Mustapic, M.; Chawla, S.; Kapogiannis, D. Plasma neuronal exosomes serve as biomarkers of cognitive impairment in HIV infection and Alzheimer's diseas. *J. Neurovirol.* **2019**, *25*, 702−709.
(17) Moos, M.; Tacke, R.; Scherer, H.; Teplow, D.; Früh, K.; Schachner, M. Neural adhesion molecule L1 as a member of the immunoglobulin superfamily with binding domains similar to fibronectin. *Nature* **1988**, *334*, 701−703.
(18) Herron, L. R.; Hill, M.; Davey, F.; Gunn-Moore, F. J. The intracellular interactions of the L1 family of cell adhesion molecules. *Biochem. J.* **2009**, *419*, 519−531.
(19) Norman, M.; Ter-Ovanesyan, D.; Trieu, W.; Lazarovits, R.; Kowal, E. J. K.; Lee, J. H.; Chen-Plotkin, A. S.; Regev, A.; Church, G. M.; Walt, D. R. L1CAM is not associated with extracellular vesicles in human cerebrospinal fluid or plasma. *Nat. Methods* **2021**, *18*, 631−634.
(20) Gomes, D. E.; Witwer, K. W. L1CAM-associated extracellular vesicles: A systematic review of nomenclature, sources, separation, and characterization. *J. Extracell. Biol.* **2022**, *1*, No. e35.
(21) Oliveira-Rodríguez, M.; López-Cobo, S.; Reyburn, H. T.; Costa-García, A.; López-Martín, S.; Yáñez-Mó, M.; Cernuda-Morollón, E.; Paschen, A.; Valés-Gómez, M.; Blanco-López, M. C. Development of a rapid lateral flow immunoassay test for detection of exosomes previously enriched from cell culture medium and body fluids. *J. Extracell. Vesicles* **2016**, *5*, No. 31803.
(22) Oliveira-Rodríguez, M.; Serrano-Pertierra, E.; García, A. C.; López-Martín, S.; Yañez-Mo, M.; Cernuda-Morollón, E.; Blanco-López, M. C. Point-of-care detection of extracellular vesicles: Sensitivity optimization and multiple-target detection. *Biosens. Bioelectron.* **2017**, *87*, 38−45.
(23) Castro-Marrero, J.; Serrano-Pertierra, E.; Oliveira-Rodríguez, M.; Zaragozá, M. C.; Martínez-Martínez, A.; Blanco-López, M. C.; Alegre, J. Circulating extracellular vesicles as potential biomarkers in chronic fatigue syndrome/myalgic encephalomyelitis: an exploratory pilot study. *J. Extracell. Vesicles* **2018**, *7*, No. 1453730.
(24) Serrano-Pertierra, E.; Oliveira-Rodríguez, M.; Matos, M.; Gutiérrez, G.; Moyano, A.; Salvador, M.; Rivas, M.; Blanco-López, M. C. Extracellular Vesicles: Current Analytical Techniques for Detection and Quantification. *Biomolecules* **2020**, *10*, No. 824.
(25) Zendrini, A.; Paolini, L.; Busatto, S.; Radeghieri, A.; Romano, M.; Wauben, M. H. M.; van Herwijnen, M. J. C.; Nejsum, P.; Borup, A.; Ridolfi, A.; Montis, C.; Bergese, P. Augmented COlorimetric NANoplasmonic (CONAN) Method for Grading Purity and Determine Concentration of EV Microliter Volume Solutions. *Front. Bioeng. Biotechnol.* **2020**, *7*, No. 452.
(26) Jeppesen, D. K.; Zhang, Q.; Franklin, J. L.; Coffey, R. J. Extracellular vesicles and nanoparticles: emerging complexities. *Trends Cell Biol.* **2023**, *33*, 667−681.
(27) Johnsen, K. B.; Gudbergsson, J. M.; Andresen, T. L.; Simonsen, J. B. What is the blood concentration of extracellular vesicles? Implications for the use of extracellular vesicles as blood-borne biomarkers of cancer. *Biochim. Biophys. Acta, Rev. Cancer* **2019**, *1871*, 109−116.
(28) Maragos, C. M.; McCormick, S. P. Monoclonal Antibodies for the Mycotoxins Deoxynivalenol and 3-Acetyl-Deoxynivalenol. *Food Agric. Immunol.* **2000**, *12*, 181−192.
(29) Mateos, H.; Mallardi, A.; Serrano-Pertierra, E.; Blanco-López, M. C.; Izzi, M.; Cioffi, N.; Palazzo, G. Unusual gold nanoparticle-antibody interactions. *JCIS Open* **2023**, *11*, No. 100089.
(30) Thobhani, S.; Attree, S.; Boyd, R.; Kumarswami, N.; Noble, J.; Szymanski, M.; Porter, R. A. Bioconjugation and characterisation of gold colloid-labelled proteins. *J. Immunol. Methods* **2010**, *356*, 60−69.
(31) Turkevich, J.; Stevenson, P. C.; Hillier, J. A study of the nucleation and growth processes in the synthesis of colloidal gold. *Discuss. Faraday Soc.* **1951**, *11*, No. 55.
(32) Koppel, D. E. Analysis of Macromolecular Polydispersity in Intensity Correlation Spectroscopy: The Method of Cumulants. *J. Chem. Phys.* **1972**, *57*, 4814−4820.
(33) Casiello, M.; Catucci, L.; Fracassi, F.; Fusco, C.; Laurenza, A. G.; Di Bitonto, L.; Pastore, C.; D'Accolti, L.; Nacci, A. ZnO/Ionic Liquid Catalyzed Biodiesel Production from Renewable and Waste Lipids as Feedstocks. *Catalysts* **2019**, *9*, No. 71.

https://doi.org/10.1021/acsomega.4c09363
ACS Omega 2025, 10, 12983−12992